Tectonophysics
Available online 6 May 2022, 229390
In Press, Journal Pre-proof

Spatial and temporal stress field changes in the focal area of the 2016 Kaikōura earthquake, New Zealand: A multi-fault process interpretation

Miu Matsuno [a], Ayaka Tagami [a], Tomomi Okada [a], Satoshi Matsumoto [b], Yuta Kawamura [b], Yoshihisa Iio [c], Tadashi Sato [a], Takashi Nakayama [a], Satoshi Hirahara [a], Stephen Bannister [d], John Ristau [d], Martha K. Savage [e], Clifford H. Thurber [f], Richard H. Sibson [g]

Show more

https://doi.org/10.1016/j.tecto.2022.229390

Highlights

- Little or no coseismic change in stress orientation occurred due to the 2016 Kaikōura earthquake.
- A large differential stress value was observed prior to the Kaikōura earthquake.
- A high slip tendency prior to the earthquake was observed along the epicentral fault
- A low slip tendency prior to the earthquake was observed at the northern end of the rupture zone.

Abstract

To understand the stress controls on the occurrence of a multi-fault rupture, we estimated the crustal stress between April 2013 to December 2018, i.e., before and after the Mw7.8 Kaikōura earthquake that occurred in New Zealand on 13 November 2016. We used both the focal mechanism solutions from the temporary seismic networks and the GeoNet moment tensor solutions and selected the solutions that differed significantly from the mainshock fault planes and rakes. Then, we performed stress tensor inversions for the selected focal mechanism solutions. Using the stress tensor inversion results, we also calculated the slip tendency. Prior to the Kaikōura earthquake, the stress regime was the strike-slip type, and the maximum eigenvalue of the stress tensor (σ_1) was oriented WNW–ESE. The stress field orientation did not change significantly after the earthquake. This suggests that the stress change during the Kaikōura earthquake was too small to alter the stress orientations, implying that there may have been large differential stress prior to the Kaikōura earthquake. However, the average stress ratio in different clusters changed in two different patterns after the earthquake, suggesting possible changes in the magnitude of different components of the stress tensor, or of pore pressure in different regions. A high slip tendency was observed at the hypocentre, while a low slip tendency was observed at the northern end of the Kaikōura earthquake faults. This may suggest that the stress orientation and the stress ratio controlled the initiation and the end of the multi-fault rupture. These results corroborate previous fault propagation models.

Keywords

2016 Mw7.8 Kaikōura earthquake; Stress tensor inversion; Coseismic stress change; Differential stress; Slip tendency

Abbreviations

HASH, Hardebeck and Shearer method; RMS, root-mean-square; SHmax, maximum horizontal compressive stress

Full Text

Help

Spatial and temporal stress field changes in the focal area of the 2016 Kaikōura earthquake, New Zealand: A multi-fault process interpretation

Miu Matsuno, Ayaka Tagami, Tomomi Okada, Satoshi Matsumoto, and Yuta Kawamura Yoshihisa Iio, Tadashi Sato, Takashi Nakayama, Satoshi Hirahara, Stephen Bannister, John Ristau, Martha Savage, Clifford Thurber, Richard Sibson

Abstract

To understand the stress controls on the occurrence of a multi-fault rupture, we estimated the crustal stress between April 2013 to December 2018, i.e., before and after the Mw7.8 Kaikōura earthquake that occurred in New Zealand on 13 November 2016. We used both the focal mechanism solutions from the temporary seismic networks and the GeoNet moment tensor solutions and selected the solutions that differed significantly from the mainshock fault planes and rakes. Then, we performed stress tensor inversions for the selected focal mechanism solutions. Using the stress tensor inversion results, we also calculated the slip tendency. Prior to the Kaikōura earthquake, the stress regime was the

#This is the accepted manuscript un-proofed. Please check Published Journal Article at: https://doi.org/10.1016/j.tecto.2022.229390

strike-slip type, and the maximum eigenvalue of the stress tensor (σ_1) was oriented WNW–ESE. The stress field orientation did not change significantly after the earthquake. This suggests that the stress change during the Kaikōura earthquake was too small to alter the stress orientations, implying that there may have been large differential stress prior to the Kaikōura earthquake. However, the average stress ratio in different clusters changed in two different patterns after the earthquake, suggesting possible changes in the magnitude of different components of the stress tensor, or of pore pressure in different regions. A high slip tendency was observed at the hypocentre, while a low slip tendency was observed at the northern end of the Kaikōura earthquake faults. This may suggest that the stress orientation and the stress ratio controlled the initiation and the end of the multi-fault rupture. These results corroborate previous fault propagation models.

Keywords: 2016 Mw7.8 Kaikōura earthquake, stress tensor inversion, coseismic stress change, differential stress, slip tendency

#This is the accepted manuscript un-proofed. Please check Published Journal Article at: https://doi.org/10.1016/j.tecto.2022.229390

Spatial and temporal stress field changes in the focal area of the 2016 Kaikōura earthquake, New Zealand: A multi-fault process interpretation

Miu Matsuno, Ayaka Tagami, Tomomi Okada, Satoshi Matsumoto, and Yuta Kawamura
Yoshihisa Iio, Tadashi Sato, Takashi Nakayama, Satoshi Hirahara,
Stephen Bannister, John Ristau, Martha Savage, Clifford Thurber,
Richard Sibson

Highlights

- Little or no coseismic change in stress orientation occurred due to the 2016 Kaikōura earthquake.
- A large differential stress value was observed prior to the Kaikōura earthquake.
- A high slip tendency prior to the earthquake was observed along the epicentral fault
- A low slip tendency prior to the earthquake was observed at the northern end of the rupture zone.

Spatial and temporal stress field changes in the focal area of the 2016 Kaikōura earthquake, New Zealand: A multi-fault process interpretation

Miu Matsuno[a], Ayaka Tagami[a], Tomomi Okada[a], Satoshi Matsumoto[b], Yuta Kawamura[b], Yoshihisa Iio[c], Tadashi Sato[a], Takashi Nakayama[a], Satoshi Hirahara[a], Stephen Bannister[d], John Ristau[d], Martha K. Savage[e], Clifford H. Thurber[f], Richard H. Sibson[g]

[a] Tohoku University, Sendai, Japan, okada.t@tohoku.ac.jp

[b] Kyushu University, Nagasaki, Japan

[c] Kyoto University, Uji, Japan

[d] GNS Science, Lower Hutt, New Zealand

[e] Victoria University of Wellington, Wellington, New Zealand

[f] University of Wisconsin-Madison, Madison, United States

[g] University of Otago, Dunedin, New Zealand.

1. Introduction[1]

[1] HASH – Hardebeck and Shearer method; RMS – root-mean-square; SHmax – maximum horizontal compressive stress

#This is the accepted manuscript un-proofed. Please check Published Journal Article at:

https://doi.org/10.1016/j.tecto.2022.229390

The 2016 Kaikōura earthquake (Mw 7.8) was a highly complex earthquake and involved the rupture of over 20 faults (e.g. Litchfield et al., 2018). New Zealand is located at the plate boundary between the Pacific and Australian plates. The northern South Island, where the 2016 Kaikōura earthquake occurred, is a transition zone between the Alpine fault strike-slip plate boundary in the south and the Hikurangi trough subduction plate boundary in the north (Figure 1). Complex crustal deformation occurs there due to oblique subduction (e.g., Okada et al., 2019). Dextral strike-slip together with convergence along the southern Alpine fault is transferred onto the splaying Marlborough fault system, e.g., the Wairau, Awatere, Clarence, Kekerengu, and Hope faults (e.g, Wallace et al., 2012). The 2016 Kaikōura earthquake initiated east of the Hope fault and linked through the Jordan Thrust, the Kekerengu fault, and other lesser faults (Figure 1). Hamling et al. (2017) constructed a multi-fault slip model of the 2016 Kaikōura earthquake using geodetic data [global navigation satellite system (GNSS) and interferometric synthetic aperture radar (InSAR)], surface traces of the coseismic rupture, and coastal uplift data. The model showed that the rupture started at the southwesternmost fault (the Humps West fault, e.g., Nicol et al., 2018), extended to the east or northeast, and ended at the northeasternmost fault (the Needles fault, e.g., Kearse et al., 2018). The seismic deformation had transpressional characteristics combined with thrusting and a dextral strike-slip motion. The aftershock distributions (e.g. Lanza et al., 2019; Mouslopoulou et al., 2019; Kawamura et al., 2021; Chamberlain et al., 2021) also suggest a multi-fault origin for the earthquake. Understanding multi-fault ruptures and their spatial extent is important not only for the Kaikōura earthquake but also for other complex earthquakes or fault systems.

#This is the accepted manuscript un-proofed. Please check Published Journal Article at:

https://doi.org/10.1016/j.tecto.2022.229390

Earthquake slip is controlled by stress and rock strength (e.g., Sibson, 1992). In previous studies (e.g. Okada et al., 2019, 2020), we observed seismic low-velocity and high Vp/Vs zones in and along the earthquake focal area. Henrys et al. (2020) suggested weak area shown as high Vp/Vs anomalies in the overriding plate stop the northern extent of the 2016 Kaikōura earthquake. These could be interpreted as lithological heterogeneities and/or overpressured fluid that reduced the fault strength and promoted the occurrence of the earthquake (e.g. Rattenbury et al., 2006; Eberhart-Phillips and Bannister, 2010; Cesca et al, 2017). These results suggest a potential strength control on earthquake occurrence in the source area.

The stress state is also important for understanding the earthquake slip process. By using the stress calculated in previous studies (e.g., Townend et al., 2012), Ando and Kaneko (2018) showed the possibility that stress orientation controls the multi-fault rupture of the Kaikōura earthquake and that rupture was arrested by the unfavorably oriented northern-end faults. Ulrich et al. (2019) also suggested the possibility of stress-controlled faulting, but they also concluded that fault strength also controlled the rupture process. On the Papatea fault, Ando and Kaneko (2018) suggested its role on rupture propagation is not dominant but Ulrich et al. (2019) suggested the Papatea fault has connected the rupture from southern faults to northern faults (the Jordan thrust). For these studies, the precise stress field in the focal area of the 2016 Kaikōura earthquake is important, but previous studies of stress orientation were made only a few years before the Kaikōura earthquake (e.g. Balfour et al., 2005; Sibson et al., 2012; Townend et al., 2012). Recently, coseismic

#This is the accepted manuscript un-proofed. Please check Published Journal Article at:

https://doi.org/10.1016/j.tecto.2022.229390

and postseismic stress changes have been discussed (e.g. Hardebeck and Okada, 2018). Coseismic and postseismic slip during an earthquake should change the stress field. Depending on the ratio between the magnitude of stress change (stress drop) and the magnitude of the pre-earthquake differential stress, the rotation angle of the orientation of principal axes of the stress field is determined. For example, for the 2011 Tohoku-oki earthquake, which was a megathrust earthquake along the subducting plate boundary in NE Japan, significant coseismic changes of about 30 degrees in the maximum compressional stress axis orientation were observed, and have been interpreted as being caused by a low differential stress value before the Mw 9.0 earthquake (e.g. Hasegawa et al., 2011). In contrast, for the 2011 Mw 6.2 Christchurch earthquake, which was a crustal earthquake on the central South Island of New Zealand, no coseismic changes in stress axis orientation were observed; therefore, it was interpreted that the coseismic stress perturbation was much smaller than the pre-seismic differential stress (Townend et al., 2012). However, Holt et al. (2013) used aftershock data from a temporary seismometer deployed near the earlier and larger Mw 7.1 Darfield earthquake on the central South Island of New Zealand and found that the maximum horizontal stress directions measured from aftershock inversions in the earthquake rupture zone tended to be parallel to the rupture plane, which suggests that the Glendale Fault was either severely mis-oriented for rupture or that the stress drop during the earthquake was approximately 40% of the pre-seismic differential stress. This variation in the magnitude of differential stress could be caused by stress concentration and frictional strength (cf. Hasegawa et al., 2011; Lamb et al., 2018). The Mw 7.8 2016 Kaikōura earthquake is an important example since it might cause large

#This is the accepted manuscript un-proofed. Please check Published Journal Article at:

https://doi.org/10.1016/j.tecto.2022.229390

stress changes. Coseismic and postseismic stress changes of the 2016 Kaikōura earthquake could help to determine the magnitude of differential stress and its relationship with the tectonic circumstance in the source area.

In this study, we determined the spatiotemporal changes in the stress field caused by the 2016 Kaikōura earthquake in the northern part of the South Island of New Zealand. We also determined the stress controls on the occurrence of a multi-fault rupture based on the slip tendency using the estimated stress field.

2. Data and Methods

Data from 75 temporary seismic stations and 22 permanent GeoNet stations were used (Fig. 1) in the period of 2013–2019 before and after the Kaikōura main shock. A three-component short-period seismometer (KVS-300, KINKEI Co. Ltd., Japan) and a low power electric data logger (EDR-X7000, KINKEI Co. Ltd., Japan) were deployed (Okada et al, 2019) at each of the temporary stations. Waveform data were digitized at a sampling frequency of 250 Hz. We also used data from the contemporaneous temporary stations (period: 14 November 2016 - 13 May 2017) described by Lanza et al. (2019) and data from short-period and broadband seismometers at GeoNet stations. We manually picked the P-wave initial motions of the waveform from all the available stations and determined the focal mechanisms with more than eight P-wave polarities using the Hardebeck and Shearer (HASH) method (Hardebeck and Shearer, 2006). HASH was also used to estimate the quality of the mechanism based on the root-mean-square (RMS) difference between the

#This is the accepted manuscript un-proofed. Please check Published Journal Article at:

https://doi.org/10.1016/j.tecto.2022.229390

best solution and acceptable solutions, that is, the tightness of the acceptable mechanisms and the number of misfits in the P-wave initial motions. We only used solutions with qualities of A (RMS difference < 25° and a misfit of < 15% of the polarities) or B (RMS difference of < 35° and a misfit of < 20% of the polarities). We used hypocenter locations and the averaged 1D velocity model in the study area of Eberhart-Phillips et al. (2010) for computing take-off angles. We used both the focal mechanisms from the earthquakes recorded by the temporary network and the GeoNet moment tensor solutions that had a variance reduction > 65% (Ristau, 2013). We estimated the stress field for the period of 2013–2019 before and after the Kaikōura main shock using stress tensor inversions. Stress tensor inversion is a method to find the principal stress orientations which reproduce the slip direction of each earthquake (e.g. Michael, 1987). Confidence ranges were estimated using the bootstrap method. In the stress tensor inversion, the selection of one fault plane from the two nodal planes of the focal mechanism has some inherent issues. Vavrycuk (2014) applied the slip instability criterion for fault plane selection to achieve a confidence range that was more realistic than that of a random selection (Michael, 1987). Therefore, we adopted Vavrycuk's (2014) method to improve the stability of the solution. We also calculated the stress ratios ($R = (\sigma_1 - \sigma_2)/(\sigma_1 - \sigma_3)$), where σ_1, σ_2, and σ_3 are the maximum, intermediate, and minimum eigenvalues of the stress tensor, respectively.

We also considered the possibility that the stress field underwent a postseismic temporal change after the main shock. We calculated the stress fields in three time windows after the main shock (13–31 November 2016, 1 December 2016–31 May 2017, and 1 June 2017–

#This is the accepted manuscript un-proofed. Please check Published Journal Article at:

https://doi.org/10.1016/j.tecto.2022.229390

4 December 2019), so that the number of events in each of the three time windows was greater than 25.

If many aftershocks occur along the fault planes of the main shock, then the fault plane may bias the stress tensor inversion (e.g. Hasegawa et al., 2011). Therefore, it is necessary to use the focal mechanisms of the aftershocks and the pre-seismic (Kaikōura) earthquakes that did not occur along the main shock fault planes of the Kaikōura earthquake. Therefore, we attempted to remove the mechanism solution on the main shock fault planes using the fault model of Hamling et al. (2017) and the Kagan angle (Kagan, 1991). The Kagan angle is the three-dimensional rotation angle between the two focal mechanisms; in this study, one is the focal mechanism corresponding to each main shock fault plane and the other is the aftershock focal mechanism. In this paper, we show results derived from using focal mechanisms with Kagan angles greater than 40° from the mainshock fault plane of the nearest, sub-fault of the Hamling et al. (2017) fault model, providing that the aftershock is less than 20 km from the subfault. We also apply this procedure for the pre-seismic period in order to remove the events on the mainshock fault planes of the Kaikōura earthquake. The focal mechanisms used in this study are shown in Fig. S1. The magnitude range is from 3.1 to 6.2.

We then calculated the slip tendency (Morris et al., 1996; Neves et al., 2009) for the fault model of Hamling et al. (2017), which is a plausible fault model because it was constructed with comprehensive information from the fault area, using the stress tensor inversion results before the Kaikōura earthquake. The slip tendency is the ratio of the shear stress (τ)

＃This is the accepted manuscript un-proofed. Please check Published Journal Article at:

https://doi.org/10.1016/j.tecto.2022.229390

to the normal stress (σ).

$$\tau = k_1[(1\text{-}\phi)^2 l^2 m^2 + \phi^2 m^2 n^2 + n^2 l^2]^{\frac{1}{2}} \quad (1)$$

$$\sigma = k_1\left(\frac{\varphi+1}{2} - (1-\phi)m^2 - n^2\right) \quad (2)$$

where (l, m, n) are the direction cosines normal to the plane in the principal stress system, ϕ is $(1 - \mathrm{R})$, k_1 is $(\sigma_1 - \sigma_3)$, and the frictional coefficient is $\mu = \tan(\varphi)$.

To calculate the slip tendency, we used the results of the stress inversion (the orientations (azimuth and plunge) of σ_1, σ_2, and σ_3 and the stress ratio) for the pre-Kaikōura earthquake period. We assumed a frictional coefficient of 0.6, which is a typical value for crustal rocks (Byerlee, 1978). If we assume a small frictional coefficient of 0.35 as used in Ando and Kaneko (2018), values of slip tendency slightly increase but the increments are about less than 0.1 and the overall patterns don't change.

3. Results

3.1 Stress field and its coseismic change

We conducted the stress field analysis by dividing the hypocentres into several regions (Fig. 2). Based on the strikes of the faults from Hamling et al.'s model, we first divided all the data into two: the northern, where most of the faults strike about NE-SW, and southern clusters, where most of the faults strike about ENE-WSW. Next, we divided the northern

#This is the accepted manuscript un-proofed. Please check Published Journal Article at:

https://doi.org/10.1016/j.tecto.2022.229390

cluster, which has enough focal mechanisms to obtain a stable solution in the stress tensor inversion, into two clusters: central, including the Kekerengu Fault, which caused a significant slip during the 2016 Kaikoura earthquake, and NE clusters, including the focal area of the 2013 Cook Strait earthquake. The number of focal mechanisms required to obtain a stable solution in the stress tensor inversion was approximately 25. Therefore, in the pre-Kaikoura earthquake analysis, the southeastern and central regions were set so that the number of focal mechanisms for each region was 25. The same regions were set also for the post-Kaikoura earthquake analysis. All the focal mechanisms used for the stress inversion analysis are within the overriding plate above the plate boundary.

For all of the clusters before and after the Kaikōura earthquake, the stress field types were strike-slip (Fig. 2). The maximum horizontal stress direction was approximately WNW–ESE both before and after the Kaikōura earthquake, and the values for each cluster were similar.

During the pre-seismic period (Fig. 2a), σ_2 for all three clusters was located near the centre of the focal sphere, and a strike-slip type stress regime was obtained. The stress ratio was 0.73 (0.67–0.79), 0.77 (0.72–0.82) and 0.83 (0.73-0.93) for the NE,central and SW clusters, respectively.

During the post-seismic period using all the earthquakes (Fig. 2b), all three clusters again had σ_2 near the centre of the focal sphere, again yielding a strike-slip type stress regime. The stress ratios for the NE and central clusters were somewhat lower 0.66 (0.65–

https://doi.org/10.1016/j.tecto.2022.229390

0.67) and 0.69 (0.64-0.74), respectively, than in the preseismic period, although the confidence ranges overlapped by a small amount. The SW cluster had confidence ranges of σ_2 and σ_3 that were wider (twice for the plunge) than those of the other two clusters. The stress ratio was 0.96 (0.94–0.98), higher than the other two clusters and also higher than the same (SW) cluster prior to the earthquake.

3.2 Postseismic change

The results for the postseismic temporal change after the main shock are shown in Fig. 3. The results for period 1 (14–31 November 2016), period 2 (1 December 2016–31 May 2017) and period 3 (1 June 2017–4 December 2019) are shown in Figure 3b, 3c and 3d, respectively. The length of each time window was determined so that the number of events in each time window was at least 25. For all clusters, σ_2 was almost vertical, and a strike-slip type stress regime was obtained but for the SW cluster in period 3, the confidence ranges of σ_2 and σ_3 were wider (twice for the plunge) than those of the other clusters. The stress ratios for period 1, 2, and 3 were 0.78 (0.74–0.82), 0.59 (0.54–0.64), and 0.57 (0.52–0.62) for the NE cluster, 0.80 (0.71–0.89), 0.50 (0.35–0.65), and 0.70 (0.61–0.79) for the central cluster, and 0.94 (0.90–0.98), 0.91 (0.85–0.97) and 0.91 (0.83–0.99) for the SW cluster.

A strike-slip stress field was determined for all three windows after the main shock. This means that there were no significant temporal changes in the type of stress field after

#This is the accepted manuscript un-proofed. Please check Published Journal Article at:

https://doi.org/10.1016/j.tecto.2022.229390

the Kaikōura earthquake through 2019. However, the stress ratio changed with time. For all three clusters, the value of the stress ratio reached its maximum during period 1. For the NE and central clusters, the value of the stress ratio decreased in periods 2 and 3. For the SW cluster, the value of the stress ratio remained high in periods 2 and 3.

3.3 Detailed analysis of the SW cluster

For the SW cluster, the confidence ranges of σ_2 and σ_3 were estimated to be wider than those of the other two clusters. This suggests a spatial heterogeneity within the SW cluster. The number of aftershock focal mechanisms in the SW cluster is sufficiently large to separate into several sub-clusters. The stress field was obtained by dividing the post-seismic SW cluster into four sub-clusters: SW1, SW2, SW3, and SW4 to consider any spatial changes (Fig. 4). The stress fields were all strike-slip types, except for cluster SW2, where the stress field was intermediate between reverse and strike-slip types. The stress ratios in all sub-clusters were nearly one; in other words, σ_2 and σ_3 were nearly equal. This may explain why the two directions can switch due to a small change in stress.

3.4 Slip tendency

We show the values of the slip tendency for each sub-fault from the Hamling et al. (2017) model in Figure 5. For the Kaikōura earthquake in this study, the estimated slip tendencies varied from 0.15 to 0.90. These variations seem to depend on the orientation of the fault strike. For most of the sub-faults, the slip direction (rake) produced by the stress inversion result was consistent with the transpressional characteristics of the model (Fig. S2 and

#This is the accepted manuscript un-proofed. Please check Published Journal Article at:

https://doi.org/10.1016/j.tecto.2022.229390

Table S1), although some of fault motion (e.g., normal fault motion at the Jordan Thrust; Howell et al., 2020) could not be explained.

4. Discussion

4.1 Stress inversion

In a previous study, Townend et al. (2012) estimated the nationwide stress tensor solutions in New Zealand using focal mechanisms from January 2004 to February 2011. Townend's clusters 11, 16, and 65 were closest to the NE, central, and SW clusters used in the present study, respectively. Townend et al. (2012) found that the maximum horizontal compressive stress (SHmax) orientation was rotated from WNW–ESE to WSW–ENE from north (Townend's cluster 11) to south (cluster 65). The values of the stress ratio *R* were 0.51 (0.33–0.70 in the 80% confidence range), 0.64 (0.45–0.83), and 0.55 (0.21–0.89) for clusters 11, 16, and 65, respectively. In this study, the SHmax or σ_1 orientations were WNW–ESE for all three clusters. The values of the stress ratio were 0.73 (0.67–0.79 in the 95% confidence range), 0.77 (0.72–0.82), and 0.83 (0.73–0.93) for the NE, central, and SW clusters, respectively. The results obtained in the present study were more consistent with those of previous studies (e.g. Balfour et al., 2005; Sibson et al., 2012), although the time periods and locations of Townend et al. (2012) and the present study differed.

The absence of a coseismic change in the stress tensor orientations is consistent with shear wave splitting analyses (Graham et al., 2020), which also do not exhibit significant

#This is the accepted manuscript un-proofed. Please check Published Journal Article at:

https://doi.org/10.1016/j.tecto.2022.229390

temporal coseismic changes. This absence of coseismic change in the orientations of the stress axes suggests large differential stress ($\sigma_1 - \sigma_3$) before the earthquake occurred. A large differential stress could have been produced by strong coupling between the Australian Plate and the Pacific Plate because relatively thick overriding crust behaves purely elastic with no internal creep because of the ‘cool’ thermal regime in the subduction zone (e.g., Reyners, 1998; Lamb et al., 2018).

We estimated the lower limit of the differential stress magnitude by calculating the coseismic stress change using the Hamling et al. (2017) model with the COULOMB software package (Lin and Stein, 2004; Toda et al., 2005). We assumed a Young’s modulus of 8×10^4 MPa and a Poisson’s ratio of 0.25, which are typical values for the crust (e.g. the COULOMB software package, Mooney et al., 1998). We considered the magnitude of σ_2 to be 180 MPa (the difference between lithostatic and hydrostatic pressures), 90 MPa, and 45 MPa, and the magnitude of σ_1 to be 1.01, 1.5, 2, 3, 4, and 5 times the magnitude of σ_2. The magnitude of σ_3 was from the value of the stress ratio obtained from the stress tensor inversion results. We calculated the principal stress axes for a set of grids throughout the entire rupture area. We estimated the lower limits of ($\sigma_1 - \sigma_3$) for the absence of coseismic change within the uncertainty to be 160–220 MPa for the SW cluster, 70–80 MPa for the central cluster, and 15–45 MPa for the NE cluster.

The results show the absence of coseismic and post-seismic stress orientation changes. However, the stress ratio R may have changed. The coseismic decrease in R for the NE and central clusters can be explained by a coseismic stress drop if the magnitude of σ_1

#This is the accepted manuscript un-proofed. Please check Published Journal Article at:

https://doi.org/10.1016/j.tecto.2022.229390

decreased dominantly under transpressional deformation (e.g., Sibson, 1993) which occurred during the multi-fault process of the 2016 Kaikōura earthquake. The stress ratio changes during the post-seismic period also may be related to the post-seismic stress drop following the Kaikōura earthquake (e.g. Wallace et al., 2018). However, the increase in R in the SW cluster cannot be explained by a stress drop.

The intermediate stress regime as shown by the higher values of R for the SW cluster after the mainshock (Figures 2, 3), particularly for SW2, can be explained by two factors. One is the stress disturbance due to coseismic slip. In fact, we can produce a stress disturbance (including a reverse type stress regime) if a small differential stress of less than ~30 MPa exists locally. This disturbance can cause an increase in the stress ratio. The other is the intermediate stress regime that was present before the earthquake. This may also be consistent with the co-existence of strike-slip and reverse faults in the North Canterbury Domain (e.g. Ghisetti and Sibson, 2012).

Additionally, pore fluid pressure change might cause the stress ratio change. For example, Warren-Smith et al. (2019) found no changes in stress orientation, but significant changes in the stress ratio for intraslab earthquakes before and after slow slip events on the subduction plate boundary in the Hikurangi margin. They related changes in the stress ratio to changes in effective stress, which could be explained by fluid pressure changes. In the study area, a shear wave splitting analysis (Graham et al., 2020) suggested a pattern of cracks oriented sub-parallel to σ_1 or σ_2, in other words, oriented with their normals sub-parallel to σ_3. For a parallel pattern of cracks oriented with their normals parallel to σ_3, the

#This is the accepted manuscript un-proofed. Please check Published Journal Article at:

https://doi.org/10.1016/j.tecto.2022.229390

change in effective stress is more effective for σ_3 (as Fig. 5 d-f in Healy, 2012). Thus an increase in the stress ratio may be caused by a decrease in fluid pressure, which causes a larger increase in the effective σ_3 than in σ_1 and σ_2. Therefore the observed post-earthquake increase in R in the SW cluster could be caused by increased porosity production leading to a decrease in fluid pressure as a fixed volume of water spreads over more cracks. The very slight increase in R immediately following the mainshock could be caused by the same phenomenon, with the decrease in the two later time periods caused either by crack healing or by infiltration of more water increasing the pore fluid pressure. We speculate that the difference in behaviour between the southwest cluster and the others may relate to the character of the surface faults, which are shorter and not as well connected in the south compared to the central and northern region (Figure 1).

4.2 Slip tendency

Previous studies of slip tendency have found its correlation with fault activity. For example, Miyakawa and Otsubo (2017) showed that active faults in central and NE Japan have high slip tendencies of 0.7 or more, whereas inactive faults have low slip tendencies of 0.7 or less. We discuss the slip tendency distribution in relation with the multi-fault process of the 2016 Kaikōura earthquake (Fig. 5).

From southwest to northeast along the rupture zone, a high slip tendency of 0.7 or more was observed along the sub-faults that correspond to the hypocentre (No. 8 in Hamling's model, Humps West). This is consistent with the initiation of slip. Most of the southwestern

#This is the accepted manuscript un-proofed. Please check Published Journal Article at:

https://doi.org/10.1016/j.tecto.2022.229390

sub-faults with strike orientations of approximately NNE–SSE had high slip tendencies, although some sub-faults with different strike orientations had low slip tendencies. The Hope Fault (No. 6 and 7) apparently has a relatively large slip tendency (~0.6) but no slip during the 2016 Kaikōura earthquake. This apparent discrepancy between slip tendency and slip could be explained by the lack of re-loading due to the other recent earthquake along the Hope fault, as suggested by Ando and Kaneko (2018).

The southernmost sub-fault (No. 5, Upper Kohwai) in the central group had a relatively large slip tendency (~0.6). This means that slip could propagate from the southwestern group to the central group. The sub-fault corresponding to the Jordan thrust (No. 4) had a low slip tendency. Kaiser et al. (2017, Fig. 3) estimated the energy release using a back-projection method. They showed that in 40–70 s of slip propagation, which corresponds to slip in and around the Jordan thrust, a relatively small amount of diffuse energy was released. We infer that the sub-fault (Jordan Thrust) with a low slip tendency delayed the slip process. High slip tendencies of >0.7 were observed at sub-faults No. 2 (Kekerengu) and No. 19 (Fidget), which could connect the slip process from the central group to the northeastern group with a large slip.

We also calculated slip tendency for the additional faults; the Point Kean (Clark et al., 2017) and the Papatea (Langdridge et al., 2018) faults, which were not included in the Hamling et al. (2017) model but were discussed as a possible offshore rupture pathway as postulated by Mousloupoulou et al. (2019), Klinger et al. (2018), Ulrich et al. (2019) and Chamberlain et al. (2021). The Point Kean fault had a high slip tendency (~0.6) if it has a

#This is the accepted manuscript un-proofed. Please check Published Journal Article at:

https://doi.org/10.1016/j.tecto.2022.229390

gentle dip angle of about 35 degrees, but the Papatea fault had a low slip tendency (< 0.3). This result prefers the suggestion that the rupture path through the Papatea fault is not significant (e.g., Ando and Kaneko, 2018).

One of the lowest slip tendencies (~ 0.1) was obtained for the northernmost sub-fault (No.1, Needles). This indicates that the slip process of the Kaikōura earthquake stopped at the sub-fault with the lowest slip tendency. This is similar to the Paso Superior detachment, which was severely mis-oriented and had a lowest slip tendency, at the north-western end of the 2010 El Mayor–Cucapah earthquake in Mexico (Fletcher et al., 2016). The analysis of a multi-fault rupture using the slip tendency suggests that a slip along a mis-oriented fault with a low slip tendency could act as a connecting fault with a high slip tendency (e.g. Fletcher et al., 2016; Quigley et al., 2018). In the case of the Kaikōura earthquake, the effect of slip along the Needles fault was insufficient to extend the rupture process further northeast.

5. Conclusions

We estimated the crustal stress before and after the Kaikōura earthquake in New Zealand. For the period before the earthquake, the stress regime was a strike-slip type, and σ_1 (or SHmax) was oriented WNW–ESE. This orientation is consistent with the results of previous studies. There were no significant temporal stress orientation changes related to the Kaikōura earthquake. A large differential stress that was present before the earthquake

#This is the accepted manuscript un-proofed. Please check Published Journal Article at:

https://doi.org/10.1016/j.tecto.2022.229390

could explain the absence of coseismic stress orientation changes. However, there were significant changes in stress ratio R in the southwestern region.

We calculated the slip tendency using the stress tensor inversion results. At the hypocentre, a high slip tendency was observed. The fault corresponding to the Jordan thrust had a low slip tendency, but the rupture process propagated to the surrounding faults with high slip tendencies. The northern end of the Kaikōura earthquake faults had the lowest slip tendency, which caused the rupture process to stop. This suggests that pre-seismic stress could explain the slip process of the Kaikōura earthquake.

The information on stress obtained in the present study will be useful as a resource for other related studies on earthquakes, faults, and tectonics. Our results suggest that complex fault processes can be controlled by stress. However, it should be noted that the present study only showed results from one earthquake. Similar analyses of other complex earthquakes are required to understand multi-fault rupture processes and their variation among earthquakes.

Funding: This study was supported by the Ministry of Education, Culture, Sports, Science and Technology (MEXT) of Japan, under its Observation and Research Program for Prediction of Earthquakes and Volcanic Eruptions. This work was also conducted with the support of a Grant-in-Aid for Special Purposes (15H05206) from MEXT, Japan, and with funding from the New Zealand Earthquake Commission (projects 18/753 and 18/755), and from the US National Science Foundation (EAR ‐ 1717119 and EAR ‐ 1756075). This

#This is the accepted manuscript un-proofed. Please check Published Journal Article at:

https://doi.org/10.1016/j.tecto.2022.229390

work was partly conducted with the support of the Scientific Research Program on Innovative Areas, ‘‘Crustal Dynamics”, at Kyoto University (2608). We used data from GeoNet.

Declaration of competing interest: The authors declare no conflict of interest.

Acknowledgements: We gratefully acknowledge the many farming communities in Nelson, Marlborough, and Canterbury, who allowed access to their land and the installation of seismic stations, as well as the Department of Conservation for granting access to Molesworth Station. Southern Geophysical Ltd. maintained and serviced the field seismic stations. Home Seismometer Corporation (Dr Shigeki Horiuchi) contributed to the waveform data processing. The program codes used in this study were provided by J. Hardebeck, V. Vavrycuk, M. C. Neves, and S. Toda. We acknowledge the seismic observation efforts of J. Pettinga, F. Ghisetti, M. Reyners, M. Kosuga, Y. Fukahata, Y. Takada, T. Miura, Y. Hamada, M. Nakamoto, M. Suzuki, K. Tateiwa, and I. Yoneda. We greatly appreciate the discussions with R. Ando, T. Matsuzawa, T. Nishimura, R. Hino, S. Toda, and Y. Yabe. We would like to thank Editage (www.editage.com) for English language editing. Finally, we are grateful to the referee and to the reviewers for their useful comments.

Data availability: The data supporting the findings of this study are available from the

＃This is the accepted manuscript un-proofed. Please check Published Journal Article at:

https://doi.org/10.1016/j.tecto.2022.229390

corresponding author, Tomomi Okada, upon request.

#This is the accepted manuscript un-proofed. Please check Published Journal Article at:

https://doi.org/10.1016/j.tecto.2022.229390

References

Ando, R., Kaneko, Y., 2018. Dynamic Rupture Simulation Reproduces Spontaneous Multifault Rupture and Arrest During the 2016 M w 7.9 Kaikoura Earthquake. Geophys. Res. Lett. 2018GL080550. https://doi.org/10.1029/2018GL080550

Balfour, N.J., Savage, M.K., Townend, J., 2005. Stress and crustal anisotropy in Marlborough, New Zealand: evidence for low fault strength and structure-controlled anisotropy. Geophys. J. Int. 163, 1073–1086. https://doi.org/10.1111/j.1365-246X.2005.02783.x

Byerlee, J., 1978. Friction of rocks. Pure Appl. Geophys. PAGEOPH 116, 615–626. https://doi.org/10.1007/BF00876528

Chamberlain, C.J., Frank, W.B., Lanza, F., Townend, J., Warren-Smith, E., 2021. Illuminating the Pre-, Co-, and Post-Seismic Phases of the 2016 M7.8 Kaikōura Earthquake With 10 Years of Seismicity. J. Geophys. Res. Solid Earth 126. https://doi.org/10.1029/2021JB022304

Cesca, S., Zhang, Y., Mouslopoulou, V., Wang, R., Saul, J., Savage, M., Heimann, S., Kufner, S.-K., Oncken, O., Dahm, T., 2017. Complex rupture process of the Mw 7.8, 2016, Kaikoura earthquake, New Zealand, and its aftershock sequence. Earth Planet. Sci. Lett. 478, 110–120. https://doi.org/10.1016/j.epsl.2017.08.024

Clark, K.J., Nissen, E.K., Howarth, J.D., Hamling, I.J., Mountjoy, J.J., Ries, W.F., Jones, K., Goldstien, S., Cochran, U.A., Villamor, P., Hreinsdóttir, S., Litchfield, N.J., Mueller, C., Berryman, K.R., Strong, D.T., 2017. Highly variable coastal deformation in the 2016 M W 7.8 Kaikōura earthquake reflects rupture complexity along a transpressional plate boundary. Earth Planet. Sci. Lett. https://doi.org/10.1016/j.epsl.2017.06.048

Eberhart-Phillips, D., Bannister, S., 2010. 3-D imaging of Marlborough, New Zealand, subducted plate and strike-slip fault systems. Geophys. J. Int. 182, 73–96. https://doi.org/10.1111/j.1365-246X.2010.04621.x

Eberhart-Phillips, D., Reyners, M., Bannister, S., Chadwick, M., Ellis, S., 2010. Establishing a Versatile 3-D Seismic Velocity Model for New Zealand. Seismol. Res. Lett. 81, 992–1000. https://doi.org/10.1785/gssrl.81.6.992

Fletcher, J.M., Oskin, M.E., Teran, O.J., 2016. The role of a keystone fault in triggering the complex El Mayor–Cucapah earthquake rupture. Nat. Geosci. 9, 303–307. https://doi.org/10.1038/ngeo2660

Ghisetti, F., Sibson, R., 2012. Compressional reactivation of E–W inherited normal faults in the area of the 2010–2011 Canterbury earthquake sequence. New Zeal. J. Geol. Geophys.

55, 177–184. https://doi.org/10.1080/00288306.2012.674048

Graham, K.M., Savage, M.K., Arnold, R., Zal, H.J., Okada, T., Iio, Y., Matsumoto, S., 2020. Spatio-temporal analysis of seismic anisotropy associated with the Cook Strait and Kaikōura earthquake sequences in New Zealand. Geophys. J. Int. 223, 1987–2008. https://doi.org/10.1093/gji/ggaa433

Hamling, I.J., Hreinsdóttir, S., Clark, K., Elliott, J., Liang, C., Fielding, E., Litchfield, N., Villamor, P., Wallace, L., Wright, T.J., D'Anastasio, E., Bannister, S., Burbidge, D., Denys, P., Gentle, P., Howarth, J., Mueller, C., Palmer, N., Pearson, C., Power, W., Barnes, P., Barrell, D.J.A., Van Dissen, R., Langridge, R., Little, T., Nicol, A., Pettinga, J., Rowland, J., Stirling, M., 2017. Complex multifault rupture during the 2016 M w 7.8 Kaikōura earthquake, New Zealand. Science (80-.). 356, eaam7194. https://doi.org/10.1126/science.aam7194

Hardebeck, J.L., Okada, T., 2018. Temporal Stress Changes Caused by Earthquakes: A Review. J. Geophys. Res. Solid Earth 123, 1350–1365. https://doi.org/10.1002/2017JB014617

Hasegawa, A., Yoshida, K., Okada, T., 2011. Nearly complete stress drop in the 2011 M w 9.0 off the Pacific coast of Tohoku Earthquake. Earth, Planets Sp. 63, 703–707. https://doi.org/10.5047/eps.2011.06.007

Healy, D., 2012. Anisotropic poroelasticity and the response of faulted rock to changes in pore-fluid pressure. Geol. Soc. London, Spec. Publ. 367, 201–214. https://doi.org/10.1144/SP367.14

Henrys, S., Eberhart-Phillips, D., Bassett, D., Sutherland, R., Okaya, D., Savage, M., Evanzia, D., Stern, T., Sato, H., Mochizuki, K., Iwasaki, T., Kurashimo, E., Seward, A., Wech, A., 2020. Upper Plate Heterogeneity Along the Southern Hikurangi Margin, New Zealand. Geophys. Res. Lett. 47. https://doi.org/10.1029/2019GL085511

Holt, R.A., Savage, M.K., Townend, J., Syracuse, E.M., Thurber, C.H., 2013. Crustal stress and fault strength in the Canterbury Plains, New Zealand, Earth and Planetary Science Letters.

Howell, A., Nissen, E., Stahl, T., Clark, K., Kearse, J., Van Dissen, R., Villamor, P., Langridge, R., Jones, K., 2020. Three-Dimensional Surface Displacements During the 2016 M W 7.8 Kaikōura Earthquake (New Zealand) From Photogrammetry-Derived Point Clouds. J. Geophys. Res. Solid Earth 125. https://doi.org/10.1029/2019JB018739

Kagan, Y.Y., 1991. 3-D rotation of double-couple earthquake sources. Geophys. J. Int. 106, 709–716. https://doi.org/10.1111/j.1365-246X.1991.tb06343.x

Kaiser, A., Balfour, N., Fry, B., Holden, C., Litchfield, N., Gerstenberger, M., D'Anastasio, E., Horspool, N., McVerry, G., Ristau, J., Bannister, S., Christophersen, A., Clark, K., Power, W., Rhoades, D., Massey, C., Hamling, I., Wallace, L., Mountjoy, J., Kaneko, Y., Benites, R., Van Houtte, C., Dellow, S., Wotherspoon, L., Elwood, K., Gledhill, K., 2017. The 2016 Kaikōura, New Zealand, Earthquake: Preliminary Seismological Report. Seismol. Res. Lett. 88, 727–739. https://doi.org/10.1785/0220170018

Kawamura, Y., Matsumoto, S., Okada, T., Matsuno, M., Iio, Y., Sato, T., Bannister, S., Ristau, J., Savage, M.K., Sibson, R.H., 2021. Characteristic of fault geometry and the subducting plate boundary in the focal area of the 2016 Mw7.8 Kaikoura earthquake, New Zealand inferred from high precision aftershock distribution, in: Japan Geoscience Union Meeting.

Klinger, Y., Okubo, K., Vallage, A., Champenois, J., Delorme, A., Rougier, E., Lei, Z., Knight, E.E., Munjiza, A., Satriano, C., Baize, S., Langridge, R., Bhat, H.S., 2018. Earthquake Damage Patterns Resolve Complex Rupture Processes. Geophys. Res. Lett. 45, 10,279-10,287. https://doi.org/10.1029/2018GL078842

Kearse, J., Little, T.A., Van Dissen, R.J., Barnes, P.M., Langridge, R., Mountjoy, J., Ries, W., Villamor, P., Clark, K.J., Benson, A., Lamarche, G., Hill, M., Hemphill-Haley, M., 2018. Onshore to Offshore Ground-Surface and Seabed Rupture of the Jordan–Kekerengu–Needles Fault Network during the 2016 Mw 7.8 Kaikōura Earthquake, New Zealand. Bull. Seismol. Soc. Am. 108, 1573–1595. https://doi.org/10.1785/0120170304

Lamb, S., Arnold, R., Moore, J.D.P., 2018. Locking on a megathrust as a cause of distributed faulting and fault-jumping earthquakes. Nat. Geosci. 11, 871–875. https://doi.org/10.1038/s41561-018-0230-5

Langridge, R.M., Rowland, J., Villamor, P., Mountjoy, J., Townsend, D.B., Nissen, E., Madugo, C., Ries, W.F., Gasston, C., Canva, A., Hatem, A.E., Hamling, I., 2018. Coseismic Rupture and Preliminary Slip Estimates for the Papatea Fault and Its Role in the 2016 Mw 7.8 Kaikōura, New Zealand, Earthquake. Bull. Seismol. Soc. Am. 108, 1596–1622. https://doi.org/10.1785/0120170336

Lanza, F., Chamberlain, C.J., Jacobs, K., Warren-Smith, E., Godfrey, H.J., Kortink, M., Thurber, C.H., Savage, M.K., Townend, J., Roecker, S., Eberhart-Phillips, D., 2019. Crustal fault connectivity of the Mw 7.8 2016 Kaikōura earthquake constrained by aftershock relocations. Geophys. Res. Lett. 2019GL082780. https://doi.org/10.1029/2019GL082780

Lin, J., Stein, R.S., 2004. Stress triggering in thrust and subduction earthquakes and stress interaction between the southern San Andreas and nearby thrust and strike-slip faults. J. Geophys. Res. Solid Earth 109. https://doi.org/10.1029/2003JB002607

Litchfield, N.J., Villamor, P., van Dissen, R.J., Nicol, A., Barnes, P.M., Barrell, D.J.A., Pettinga, J.R., Langridge, R.M., Little, T.A., Mountjoy, J.J., Ries, W.F., Rowland, J., Fenton, C., Stirling, M.W., Kearse, J., Berryman, K.R., Cochran, U.A., Clark, K.J., Hemphill-Haley, M., Khajavi, N., Jones, K.E., Archibald, G., Upton, P., Asher, C., Benson, A., Cox, S.C., Gasston, C., Hale, D., Hall, B., Hatem, A.E., Heron, D.W., Howarth, J., Kane, T.J., Lamarche, G., Lawson, S., Lukovic, B., McColl, S.T., Madugo, C., Manousakis, J., Noble, D., Pedley, K., Sauer, K., Stahl, T., Strong, D.T., Townsend, D.B., Toy, V., Williams, J., Woelz, S., Zinke, R., 2018. Surface rupture of multiple crustal faults in the 2016 Mw 7.8 Kaikōura, New Zealand, earthquake. Bull. Seismol. Soc. Am. 108, 1496–1520. https://doi.org/10.1785/0120170300

Michael, A.J., 1987. Use of focal mechanisms to determine stress: A control study. J. Geophys. Res. 92, 357. https://doi.org/10.1029/JB092iB01p00357

Miyakawa, A., Otsubo, M., 2017. Evolution of crustal deformation in the northeast-central Japanese island arc: Insights from fault activity. Isl. Arc 26, e12179. https://doi.org/10.1111/iar.12179

Mooney, W.D., Laske, G., Masters, T.G., 1998. CRUST 5.1: A global crustal model at 5° × 5°. J. Geophys. Res. Solid Earth 103, 727–747. https://doi.org/10.1029/97JB02122

Morris, A., Ferrill, D.A., Brent Henderson, D.B., 1996. Slip-tendency analysis and fault reactivation. Geology 24, 275. https://doi.org/10.1130/0091-7613(1996)024<0275:STAAFR>2.3.CO;2

Mouslopoulou, V., Saltogianni, V., Nicol, A., Oncken, O., Begg, J., Babeyko, A., Cesca, S., Moreno, M., 2019. Breaking a subduction-termination from top to bottom: The large 2016 Kaikōura Earthquake, New Zealand. Earth Planet. Sci. Lett. 506, 221–230. https://doi.org/10.1016/j.epsl.2018.10.020

Nicol, A., Khajavi, N., Pettinga, J.R., Fenton, C., Stahl, T., Bannister, S., Pedley, K., Hyland-Brook, N., Bushell, T., Hamling, I., Ristau, J., Noble, D., McColl, S.T., 2018. Preliminary Geometry, Displacement, and Kinematics of Fault Ruptures in the Epicentral Region of the 2016 Mw 7.8 Kaikōura, New Zealand, Earthquake. Bull. Seismol. Soc. Am. 108, 1521–1539. https://doi.org/10.1785/0120170329

Neves, M.C., Paiva, L.T., Luis, J., 2009. Software for slip-tendency analysis in 3D: A plug-in for Coulomb. Comput. Geosci. 35, 2345–2352. https://doi.org/10.1016/j.cageo.2009.03.008

Okada, T., Iio, Y., Matsumoto, S., Bannister, S., Ohmi, S., Horiuchi, S., Sato, T., Miura, T., Pettinga, J., Ghisetti, F., Sibson, R.H., 2019. Comparative tomography of reverse-slip and strike-slip seismotectonic provinces in the northern South Island, New Zealand.

Tectonophysics 765, 172–186. https://doi.org/10.1016/j.tecto.2019.03.016

Okada, T., Matsuno, M., Matsumoto, S., Kawamura, Y., Iio, Y., Sato, T., Nakayama, T., Hirahara, S., Bannister, S., Ristau, J., Savage, M.K., Thurber, C.H., Sibson, R.H., 2021. Complexity of the 2016 M 7.8 Kaikoura, New Zealand, earthquake from seismic observation: inferences of overpressured fluid involvement. Tectonophysics submitted.

Okada, T., Matsuno, M., Matsumoto, S., Kawamura, Y., Iio, Y., Sato, T., Nakayama, T., Hirahara, S., Bannister, S., Ristau, J., Savage, M.K., Thurber, C.H., Sibson, R.H., 2020. Possible involvement of overpressured fluid in multi-faut rupture inferred from seismic observations of the 2016 Kaikoura earthquake, in: Annual Conference of Geoscience Society of New Zealand.

Quigley, M.C., Jiménez, A., Duffy, B., King, T.R., 2019. Physical and Statistical Behavior of Multifault Earthquakes: Darfield Earthquake Case Study, New Zealand. J. Geophys. Res. Solid Earth 2019JB017508. https://doi.org/10.1029/2019JB017508

Rattenbury, M., Townsend, D.B., Johnston, M.., 2006. Geology of the Kaikoura area. IGNS 1250,000 Geol. Map 13.

Reyners, M., 1998. Plate coupling and the hazard of large subduction thrust earthquakes at the Hikurangi subduction zone, New Zealand. New Zeal. J. Geol. Geophys. 41, 343–354. https://doi.org/10.1080/00288306.1998.9514815

Ristau, J., 2013. Update of Regional Moment Tensor Analysis for Earthquakes in New Zealand and Adjacent Offshore Regions. Bull. Seismol. Soc. Am. 103, 2520–2533. https://doi.org/10.1785/0120120339

Sibson, R.H., Ghisetti, F.C., Crookbain, R. a., 2012. Andersonian wrench faulting in a regional stress field during the 2010-2011 Canterbury, New Zealand, earthquake sequence. Geol. Soc. London, Spec. Publ. 367, 7–18. https://doi.org/10.1144/SP367.2

Sibson, R.H., 1992. Implications of fault-valve behaviour for rupture nucleation and recurrence. Tectonophysics 211, 283–293. https://doi.org/10.1016/0040-1951(92)90065-E

Sibson, R.H., 1993. Load-strengthening versus load-weakening faulting. J. Struct. Geol. 15, 123–128. https://doi.org/10.1016/0191-8141(93)90090-W

Toda, S., Stein, R.S., Richards-Dinger, K.B., Bozkurt, S., 2005. Forecasting the evolution of seismicity in southern California: Animations built on earthquake stress transfer. J. Geophys. Res. 110, B05S16. https://doi.org/10.1029/2004JB003415

Townend, J., Sherburn, S., Arnold, R., Boese, C., Woods, L., 2012. Three-dimensional variations in present-day tectonic stress along the Australia–Pacific plate boundary in New Zealand. Earth Planet. Sci. Lett. 353–354, 47–59.

https://doi.org/10.1016/j.epsl.2012.08.003

Ulrich, T., Gabriel, A.-A., Ampuero, J.-P., Xu, W., 2019. Dynamic viability of the 2016 Mw 7.8 Kaikōura earthquake cascade on weak crustal faults. Nat. Commun. 10, 1213. https://doi.org/10.1038/s41467-019-09125-w

Vavryčuk, V., 2014. Iterative joint inversion for stress and fault orientations from focal mechanisms. Geophys. J. Int. 199, 69–77. https://doi.org/10.1093/gji/ggu224

Wallace, L.M., Barnes, P., Beavan, J., Van Dissen, R., Litchfield, N., Mountjoy, J., Langridge, R., Lamarche, G., Pondard, N., 2012. The kinematics of a transition from subduction to strike-slip: An example from the central New Zealand plate boundary. J. Geophys. Res. 117, B02405. https://doi.org/10.1029/2011JB008640

Wallace, L.M., Hreinsdóttir, S., Ellis, S., Hamling, I., D'Anastasio, E., Denys, P., 2018. Triggered Slow Slip and Afterslip on the Southern Hikurangi Subduction Zone Following the Kaikōura Earthquake. Geophys. Res. Lett. https://doi.org/10.1002/2018GL077385

Warren-Smith, E., Fry, B., Wallace, L., Chon, E., Henrys, S., Sheehan, A., Mochizuki, K., Schwartz, S., Webb, S., Lebedev, S., 2019. Episodic stress and fluid pressure cycling in subducting oceanic crust during slow slip. Nat. Geosci. https://doi.org/10.1038/s41561-019-0367-x

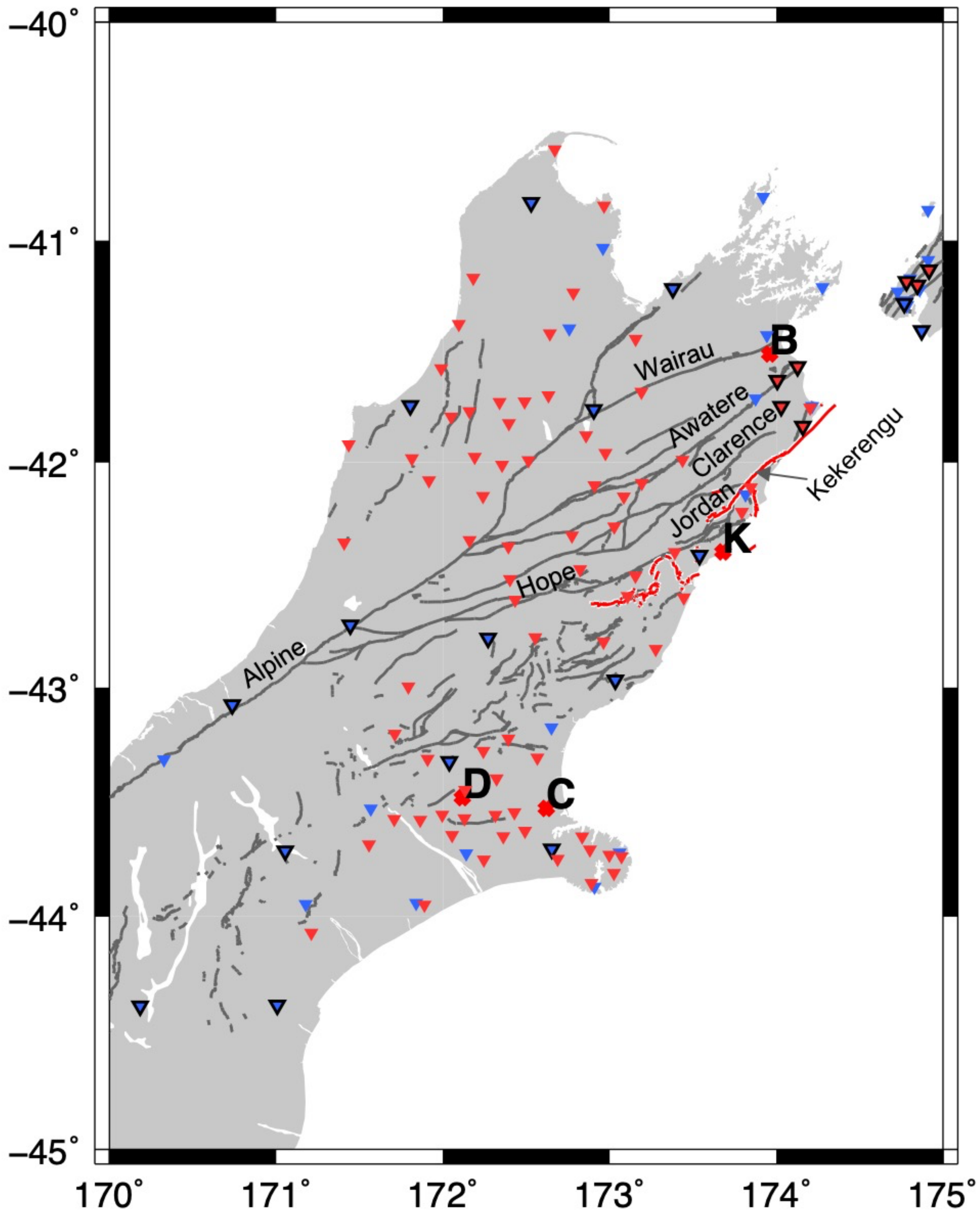

Fig. 1. Station map. Blue triangles with and without outline indicate permanent (GeoNet) stations with broadband and short-period seismometers, respectively. Red triangles with and without outline show temporary stations from Lanza et al. (2019) and Okada et al. (2019), respectively. Grey and red lines indicate the surface traces of active faults and the 2016 Kaikōura earthquake, respectively. Red bold crosses with capitals show the location of towns; B: Blenheim, C: Christchurch, D: Darfield, K: Kaikoura.

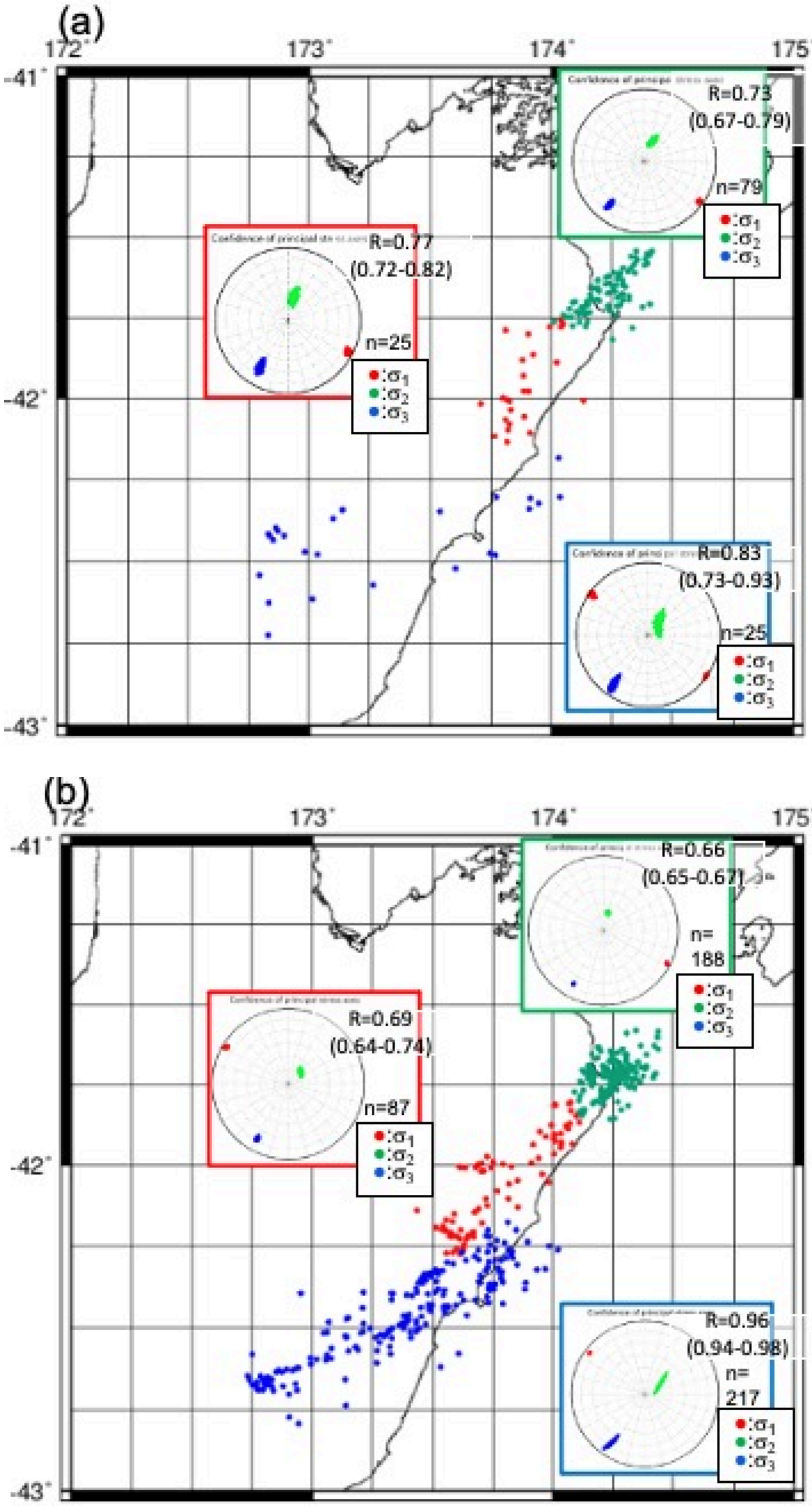

Fig. 2. Result of stress tensor inversion. Fig. 1 (a) Before and (b) after the Kaikoura earthquake. The results are shown using lower hemisphere projections. Red, green, and blue circles within the stress tensor inversions denote the 95% confidence ranges of σ_1, σ_2, and σ_3, respectively. The value of the stress ratio ($R = (\sigma_1 - \sigma_2)/(\sigma_1 - \sigma_3)$) is also shown. Numbers in parentheses indicate the 95% confidence range of R. After "n=," the number of focal mechanisms used for each stress tensor inversion is shown. Map shows the distribution of earthquakes (green, red and orange keyed for each cluster with the corresponding color box outlining the stress inversion results.

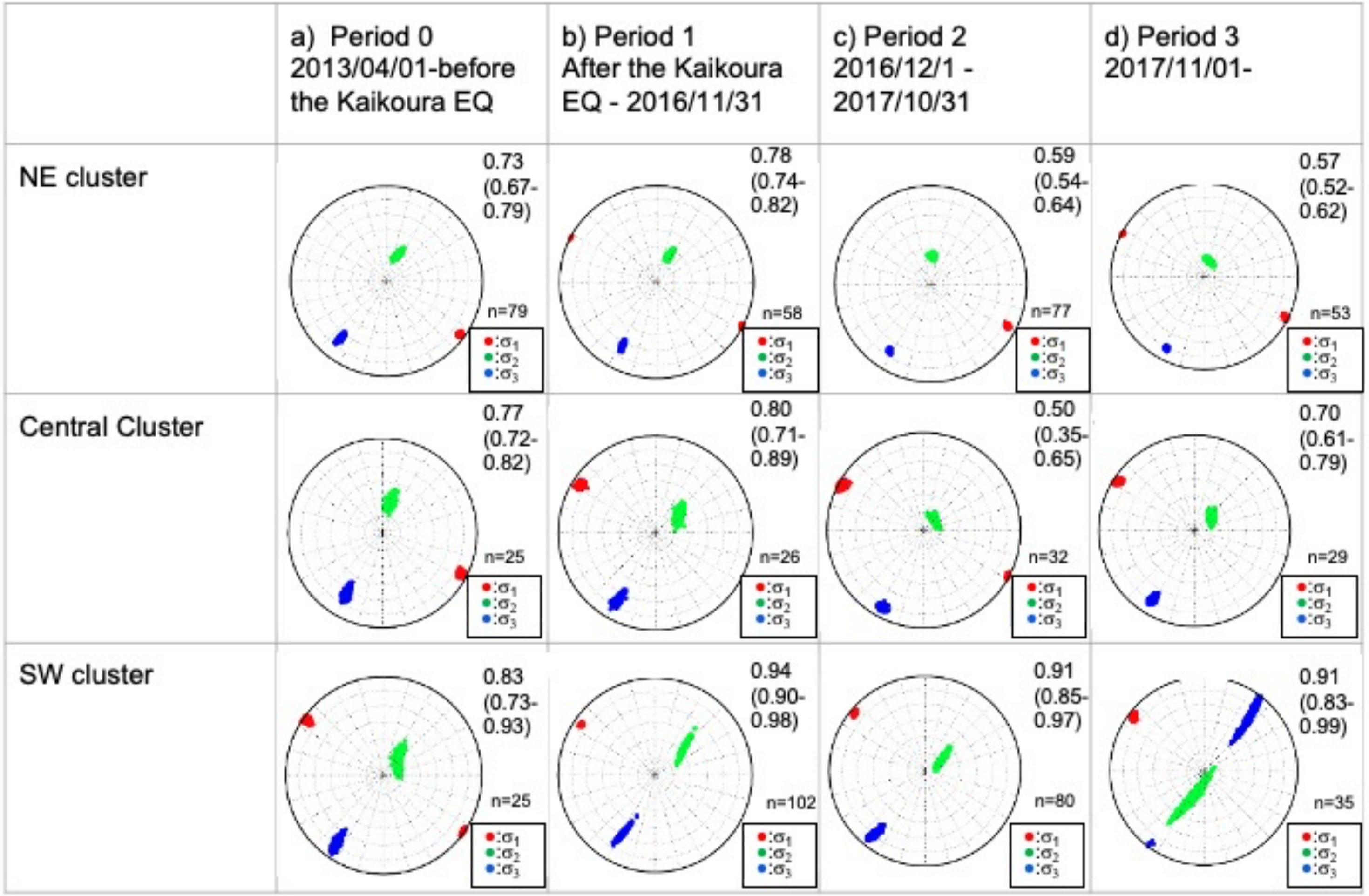

Fig. 3. Temporal change in the stress tensor inversion result. Numbers are the values of the stress ratio. The results are shown using lower hemisphere projections. Red, green, and blue denote the 95% confidence interval of σ1, σ2, and σ3, respectively. The value of the stress ratio (R = (σ1 − σ2)/(σ1 − σ3)) is also shown. Numbers in parentheses show the 95% confidence range of R. After “n=,” the number of focal mechanisms used for each stress tensor inversion is shown.

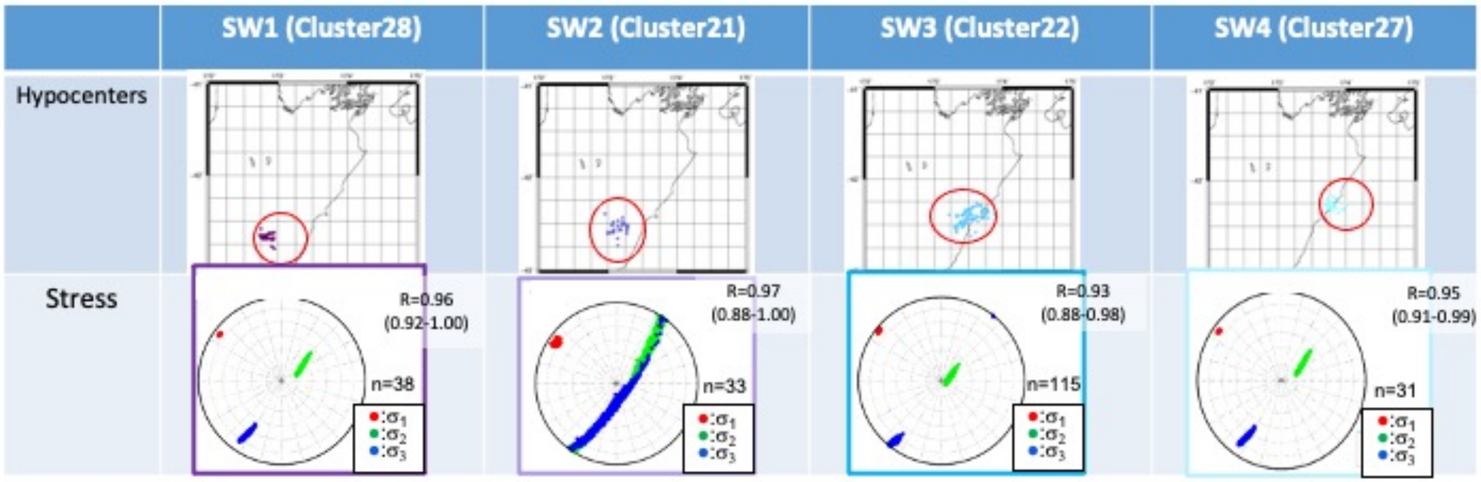

Fig. 4. Result of the stress tensor inversion for sub-clusters in the southwestern part of the aftershock area. The results are shown using lower hemisphere projections. Red, green, and blue denote the 95% confidence interval of σ_1, σ_2, and σ_3, respectively. The value of the stress ratio ($R = (\sigma_1 - \sigma_2)/(\sigma_1 - \sigma_3)$) is also shown. Numbers in parentheses show the 95% confidence range of R. After "n=," the number of focal mechanisms used for each stress tensor inversion is shown.

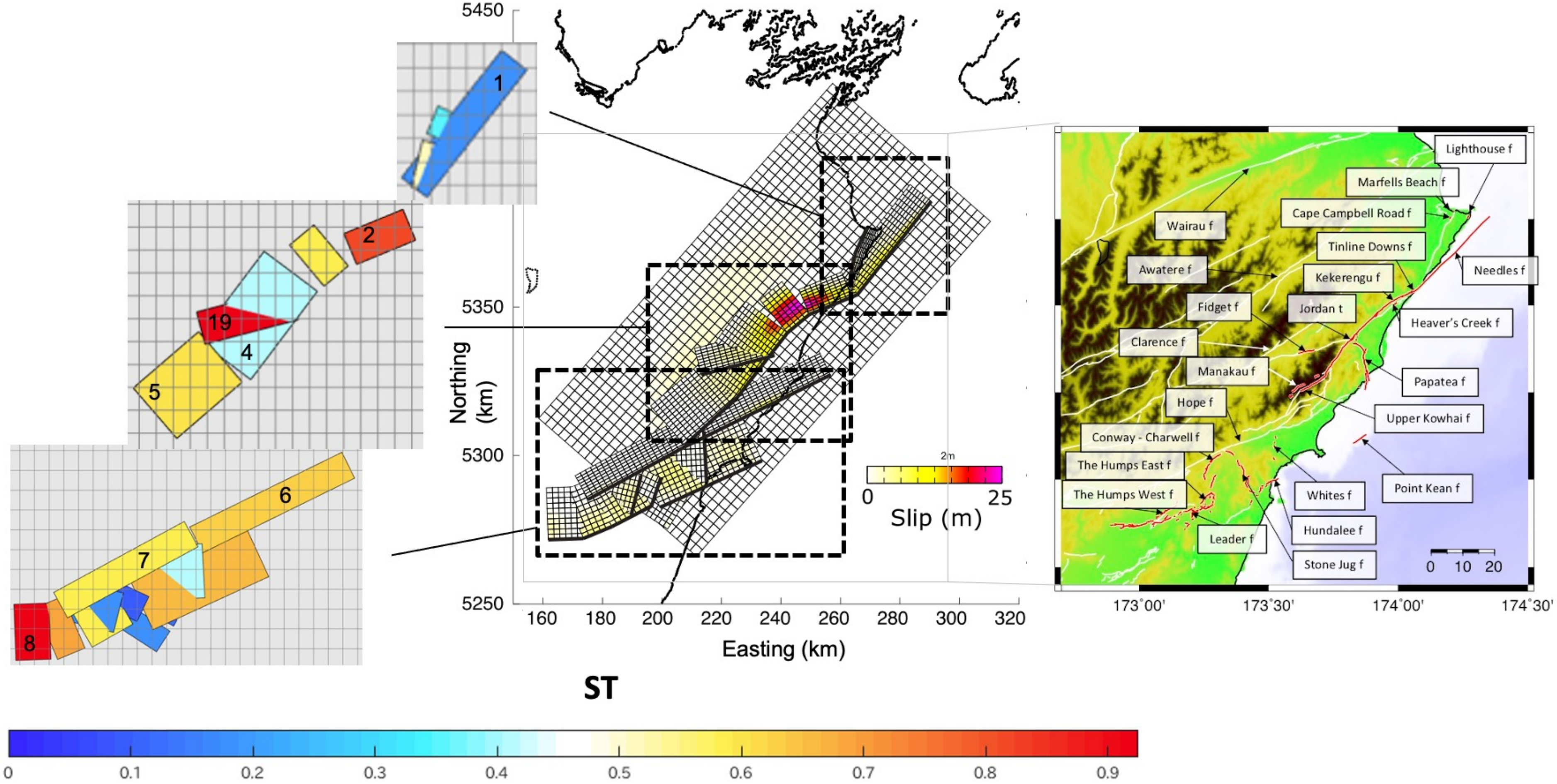

Fig. 5. Left: Result of the slip tendency calculations. Colours indicate the value of the slip tendency for each sub-fault. Numbers are from the fault numbers of Hamling et al. (2017); See text for details. Middle: figure is slip distribution by Hamling et al. (2017, Fig. 6A). Right: Surface ruptures of the Kaikōura earthquake (from Litchfield et al., 2018, Fig. 1).

Spatial and temporal stress field changes in the focal area of the 2016 Kaikōura earthquake, New Zealand: A multi-fault process interpretation

Miu Matsuno, Ayaka Tagami, Tomomi Okada, Satoshi Matsumoto, and Yuta Kawamura
Yoshihisa Iio, Tadashi Sato, Takashi Nakayama, Satoshi Hirahara,
Stephen Bannister, John Ristau, Martha Savage, Clifford Thurber,
Richard Sibson

Supplementary Materials

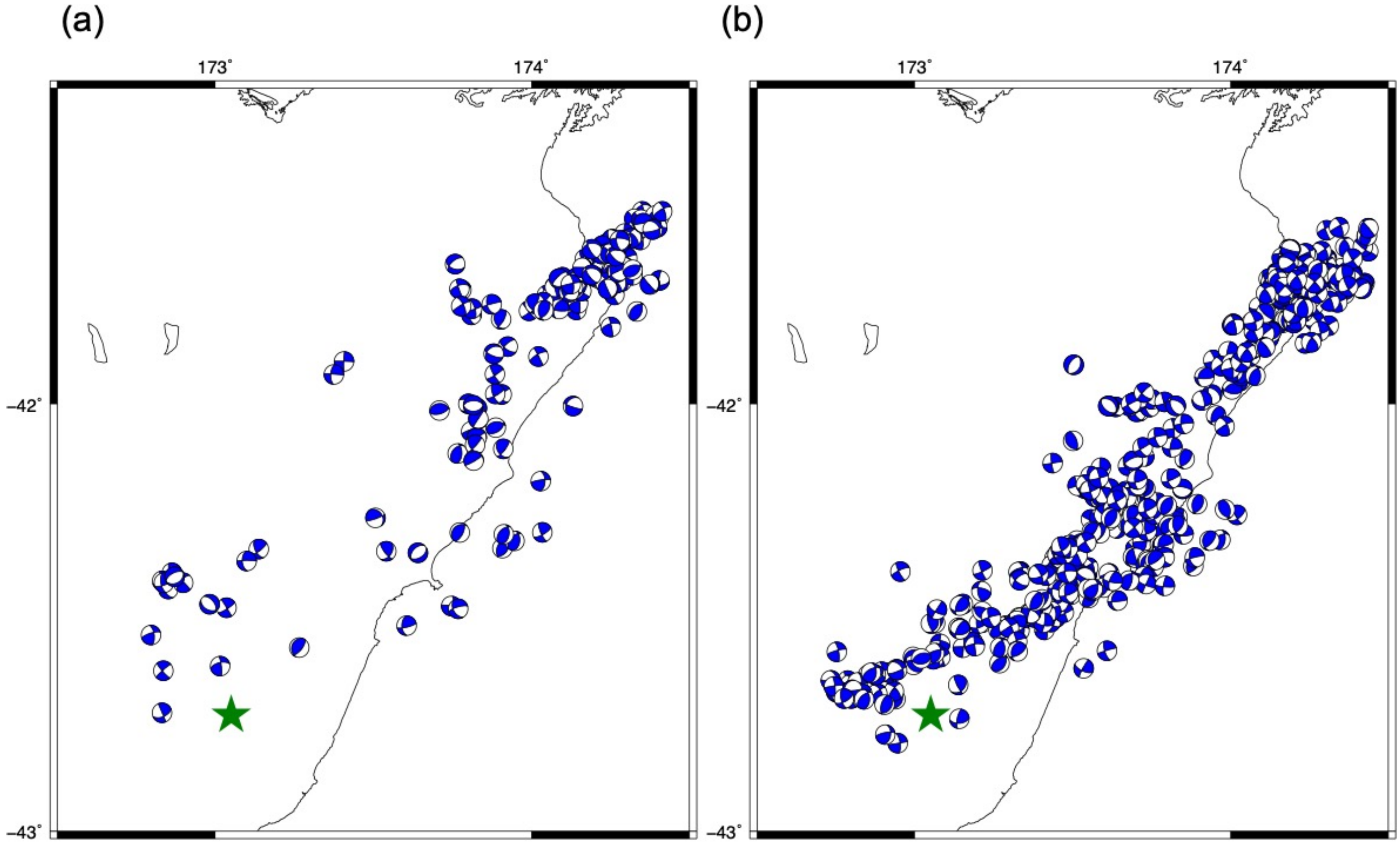

Fig. S1. Focal mechanisms obtained in this study. (a) Before and (b) after the Kaikōura earthquake. Focal mechanisms are shown using lower hemisphere projections. The star denotes the hypocentre of the mainshock.

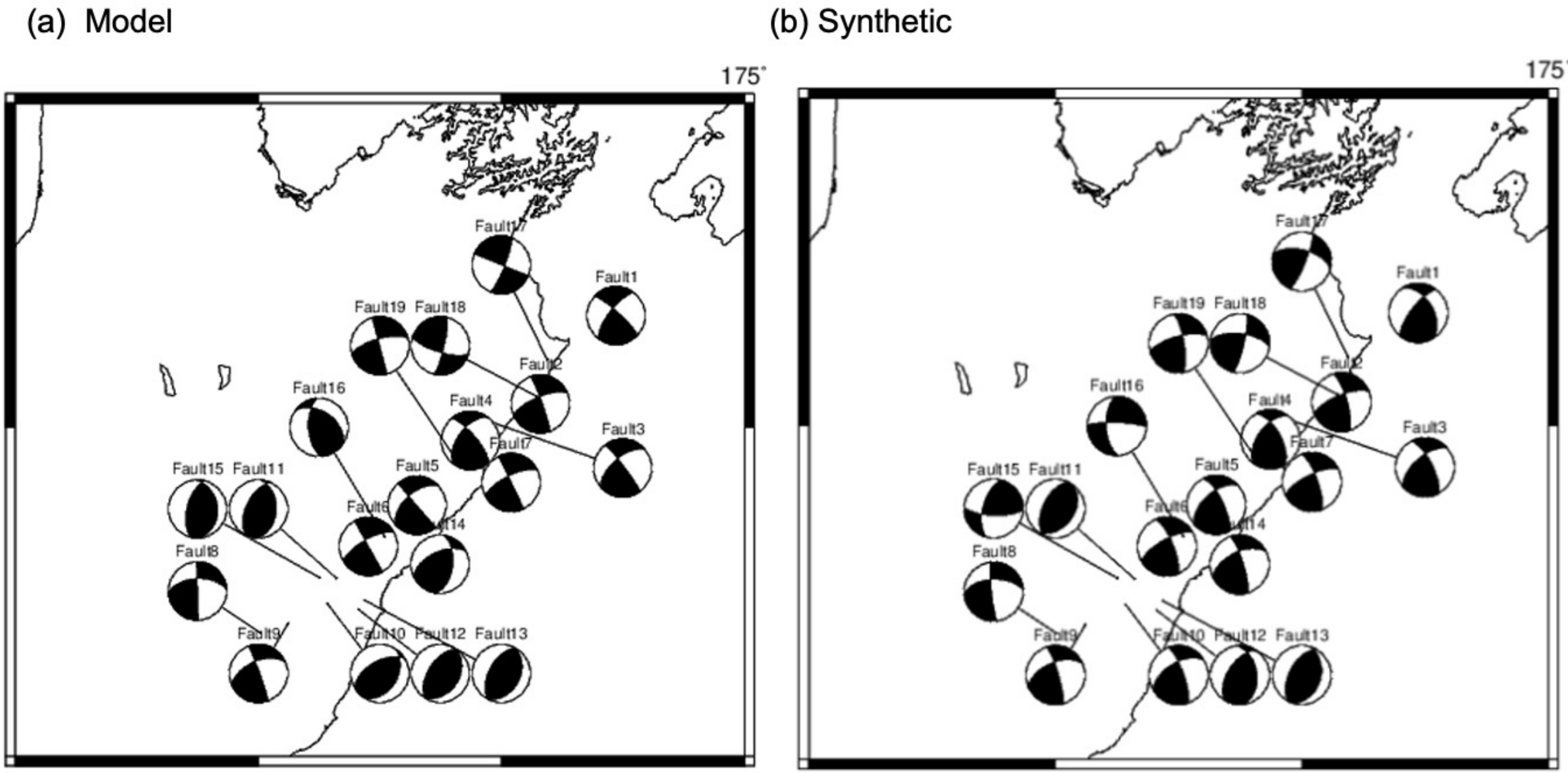

Fig. S2. Comparisons of slip along each fault (a) using Hamling's model and (b) using the results of the stress tensor inversion. Focal mechanisms are shown using lower hemisphere projections. Fault numbers are from Hamling et al. (2017).

	Longitude	Latitude	Strike (°)	Dip (°)	Rake_Model (°)	Rake_SI (°)
Fault1	174.4715	−41.6568	218	70	169	134
Fault2	174.1606	−41.9284	248	70	174	163
Fault3	173.9624	−41.9846	230	60	174	156
Fault4	173.872	−42.0403	217	55	159	143
Fault5	173.6521	−42.2387	229	55	180	155
Fault6	173.4537	−42.3641	241	70	180	162
Fault7	174.0407	−42.1693	244	70	180	163
Fault8	173.0075	−42.6266	268	55	180	187
Fault9	173.1227	−42.5984	247	55	175	169
Fault10	173.2851	−42.5381	240	55	107	163
Fault11	173.3212	−42.4611	205	55	103	83
Fault12	173.4116	−42.5558	213	55	90	116
Fault13	173.4352	−42.5274	208	55	90	96
Fault14	173.7472	−42.4182	245	55	133	167
Fault15	173.2535	−42.4594	194	60	100	22
Fault16	173.5205	−42.335	177	60	124	350
Fault17	174.1875	−41.7916	22	80	180	33
Fault18	174.1451	−41.905	13	80	162	28
Fault19	173.8161	−42.1024	255	70	180	164

Table S1. Comparison of rakes from the Hamling et al. (2017) model (Rake_Model), and the calculations using the stress tensor inversion results (Rake_SI). Longitude and latitude indicate the location of the fault patch with maximum slip on each sub-fault. Strike and dip are from the model.